Learning Cross-Domain Correspondence for Control with Dynamics Cycle-Consistency

Qiang Zhang*
Shanghai Jiao Tong University
Shanghai, 200240
zhangqiang2016@sjtu.edu.cn

Tete Xiao
UC Berkeley
Berkeley, CA 94720
txiao@eecs.berkeley.edu

Alexei A. Efros
UC Berkeley
Berkeley, CA 94720
efros@eecs.berkeley.edu

Lerrel Pinto
New York University
New York, NY 10003
lerrel@cs.nyu.edu

Xiaolong Wang
UC San Diego
San Diego, CA 92093
xiw012@ucsd.edu

Abstract

At the heart of many robotics problems is the challenge of learning correspondences across domains. For instance, imitation learning requires obtaining correspondence between humans and robots; sim-to-real requires correspondence between physics simulators and real hardware; transfer learning requires correspondences between different robot environments. In this paper, we propose to learn correspondence across such domains emphasizing on differing modalities (vision and internal state), physics parameters (mass and friction), and morphologies (number of limbs). Importantly, correspondences are learned using unpaired and randomly collected data from the two domains. We propose *dynamics cycles* that align dynamic robotic behavior across two domains using a cycle consistency constraint. Once this correspondence is found, we can directly transfer the policy trained on one domain to the other, without needing any additional fine-tuning on the second domain. We perform experiments across a variety of problem domains, both in simulation and on real robots. Our framework is able to align uncalibrated monocular video of a real robot arm to dynamic state-action trajectories of a simulated arm without paired data. Video demonstrations of our results are available at :https://sites.google.com/view/cycledynamics

1 Related work

Learning invariant representations. To find cross-domain alignment, researchers have proposed to learn representations which are invariant to the changes unrelated to downstream tasks [Tobin et al., 2017, Peng et al., 2018, Gupta et al., 2017, Sermanet et al., 2018, Liu et al., 2017b, Pinto et al., 2017, Sadeghi and Levine, 2016, Yan et al., 2020, Andrychowicz et al., 2018]. To align two domains where the dynamics are different, Gupta et al. [2017] propose to learn invariant features by pairs of states from two domains. However, paired data is hard to collect, and the method is limited to state space, while real-world observations are often based on images [Taylor and Stone, 2009].

Learning translation. Instead of learning invariance, our method is related to works which learn the mapping across two domains for alignment [Ammar et al., 2015, Joshi and Chowdhary, 2018, Kim et al., 2019, Smith et al., 2019, Taylor et al., 2007]. Our method can learn correspondence between simulated and real robot through *unpaired and randomly collected* trajectories.

*Work done during Qiang's internship at UC Berkeley.

NeurIPS 2020 3rd Robot Learning Workshop: Grounding Machine Learning Development in the Real World.

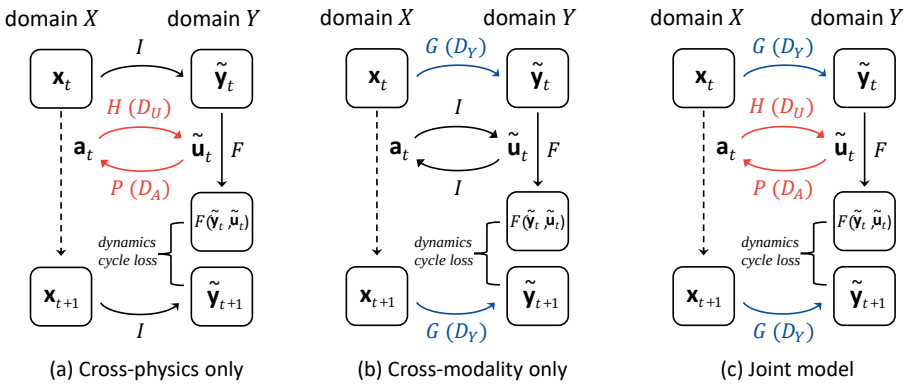

Figure 1: **Model framework**: (a) Joint model for *cross-modality-and-physics* alignment; (b) Model for only *cross-modality* alignment; (c) Model for only *cross-physics* alignment. Red arrows indicate correspondences between actions and blue arrows indicate correspondence between observations.

Cycle-Consistency. Our work is inspired by literature on cycle-consistency [Zhu et al., 2017, Liu et al., 2017a, Bansal et al., 2018, Hoffman et al., 2017, James et al., 2019, Zhou et al., 2016, Bousmalis et al., 2018]. However, all these works are restricted on visual alignments, while ours can align agents cross different dynamics and structures.

2 Introduction

Recently, an emerging line of research focuses on finding correspondences under a realistic problem setting by learning to translate between two different domains with *unpaired* data Zhu et al. [2017], Bansal et al. [2018]. While this translation technique has shown encouraging results in imitation learning Smith et al. [2019] and sim-to-real transfer James et al. [2019], Hoffman et al. [2017], it is limited to finding correspondences only in the visual observation space. However, in real-world applications, besides visual observations, the physics parameters and morphology dynamics between two domains are often unaligned. Hence, to truly extend correspondence learning to aligning behaviors, we must go beyond the image space and explicitly incorporate dynamics information.

We aim to learn correspondence across various domains, i.e., input modalities, physics parameters, and morphology. We formulate the trajectories of domain X and Y as $\tau_X \doteq (\mathbf{x}_t, \mathbf{a}_t, \mathbf{x}_{t+1})$ and $\tau_Y \doteq (\mathbf{y}_t, \mathbf{u}_t, \mathbf{y}_{t+1})$, where $\mathbf{x} \in \mathcal{R}^{n_1}$ and $\mathbf{y} \in \mathcal{R}^{n_2}$ are observation representations in domain X and Y, $\mathbf{a} \in \mathcal{R}^{m_1}$ and $\mathbf{u} \in \mathcal{R}^{m_2}$ are action representations in domain X and Y, and t is time step. Without loss of generality, we assume to learn correspondence from domain X to domain Y.

Suppose that we have observation alignment functions $G : X \mapsto Y$, and action alignment function $H : A \mapsto U$ and its inverse counterpart $H^{-1} : U \mapsto A$. We define two types of correspondence:

Observation Correspondence, i.e., what the representation of one observation in domain X should correspond to if it is in domain Y, and vice versa. For example, if X is visual sensing of an agent while Y is the state (e.g., joint angle) of the *same* agent, G functions as a state estimator. If X is the state of one agent while Y is the state of a *structurally different* agent, such as a Sawyer arm and a UR5 arm, G aligns the states at a same stage towards a common goal (in the case of robot arms the position of end effector could be the bridge). We denote two correspondent observations between X and Y as $\mathbf{x} \Leftrightarrow \mathbf{y}$.

Action Correspondence, i.e., with correspondent initial observations which actions to execute so that the next observations in two domains remain correspondent. For example, if X and Y are two environments with different physics parameters, with the initial observations $\mathbf{x}_t$, $\mathbf{y}_t$ and $\mathbf{x_t} \Leftrightarrow \mathbf{y_t}$, after action $\mathbf{a}_t$ is executed in domain X and leads to the next observation $\mathbf{x}_{t+1}$, alignment function H should find the action $\mathbf{u}_t$ which leads to next observation $\mathbf{y}_{t+1}$ in domain Y where $\mathbf{x}_{t+1} \Leftrightarrow \mathbf{y}_{t+1}$, and vice versa for H^{-1}. We denote two correspondent actions from X and Y as $(\mathbf{x}_t, \mathbf{a}_t) \Leftrightarrow (\mathbf{y}_t, \mathbf{u}_t)$.

3 Cycle Dynamics Model

We begin by simply mapping states across domains by adversarial training. Given unpaired samples $\{\mathbf{x}_i\} \in X$, and $\{\mathbf{y}_i\} \in Y$, a mapping function G can be learned with a discriminator D_Y with the adversarial objective, where G tries to map $\mathbf{x}$ onto the distribution of $\mathbf{y}$, while D_Y tries to distinguish

translated samples $G(\mathbf{x})$ against real samples y:

$$\min_{G}\max_{D_Y}\mathcal{L}_{\mathrm{adv}}\left(G,D_Y\right)=\mathbb{E}_{\mathbf{y}\sim p(\mathbf{y})}\left[\log D_Y(\mathbf{y})\right]+\mathbb{E}_{\mathbf{x}\sim p(\mathbf{x})}\left[\log\left(1-D_Y(G(\mathbf{x}))\right)\right] \tag{1}$$

The adversarial objective reaches global optimal when the mapping function G can perfectly ground the translated samples onto the distribution defined by $\{\mathrm{y}_i\}$.

We learn an action mapping function $H:A\mapsto U$ which maps actions from domain X to domain Y, and model its inverse counterpart H^{-1} as a function $P:U\mapsto A$ with separate parameters. Besides using two adversarial losses with discriminators D_U in Y and D_A in X, i.e., $\mathcal{L}_{\mathrm{adv}}(H,D_U)$ and $\mathcal{L}_{\mathrm{adv}}(P,D_A)$, we add cross-domain cycle consistency loss Zhu et al. [2017] into the objective:

$$\min_{H,P}\mathcal{L}_{\mathrm{dom\_cyc}}\left(H,P\right)=\mathbb{E}_{\mathbf{a}\sim p(\mathbf{a})}\left[P(H(\mathbf{a}))-\mathbf{a}_1\right], \tag{2}$$

which implies that the translated action should be able to be translated back, i.e., $P(H(\mathbf{a}))\approx\mathbf{a}$.

Nevertheless, the structure of learnt mapping by adversarial training is loosely constrained. Vanilla adversarial training may map all samples X to a few samples of Y, which still minimizes the adversarial objective. Adding domain cycle consistency loss does not solve the problem fundamentally: for example, given two correspondent but *unpaired* observations, i.e., $\mathbf{x}_t,\mathbf{y}_t$ and $\mathbf{x}_{t+1},\mathbf{y}_{t+1}$, G can map $\mathbf{x}_t$ to $\mathbf{y}_{t+1}$ and G^{-1} can still map $\mathbf{y}_{t+1}$ back to $\mathbf{x}_t$, which does not violate domain cycle-consistency.

Beyond only relying domain cycle consistency, we exploit the transition dynamics of two domains, termed as *dynamics cycle-consistency*. As illustrated in Figure 1(a), we map the observation-action pair at time step t $\mathbf{x}_t$ and $\mathbf{a}_t$ from domain X to Y using G and H, then execute the translated observation and action $\tilde{\mathbf{y}}_t$ and $\tilde{\mathbf{u}}_t$) in domain Y by its transition dynamics $T_Y:Y\times U\mapsto Y$ to get the next observation, which is expected to be correspondent to the next observation from domain X, i.e., $T_Y(\tilde{\mathbf{y}}_t,\tilde{\mathbf{u}}_t)\Leftrightarrow\mathbf{x}_{t+1}$. According to the definition of observation correspondence, $T_Y(\tilde{\mathbf{y}}_t,\tilde{\mathbf{u}}_t)$ should be the same as $G(\mathbf{x}_{t+1})$, as expressed in the objective:

$$\min_{G,H}\mathcal{L}(G,H)_{\mathrm{dyn\_cyc}}=\mathbb{E}_{(\mathbf{x}_t,\mathbf{a}_t,\mathbf{x}_{t+1})\sim p(\tau_X)}\left[G(\mathbf{x}_{t+1})-T_Y(G(\mathbf{x}_t),H(\mathbf{a}_t))_1\right] \tag{3}$$

One obstacle remains. The transition dynamics T_Y in Equation 3 is in fact the physical property of a simulator or the real world, hence it is not differentiable for back-propagation. In consequence, we train a forward model which takes an observation-action pair as input and predicts the next observation to approximate the dynamics of the environment. Since we have access to trajectories from Y, we can directly train the forward model using supervised regression objective:

$$\min_{F}\mathcal{L}_{\mathrm{forward}}(F)=\mathbb{E}_{(\mathbf{y}_t,\mathbf{u}_t,\mathbf{y}_{t+1})\sim p(\tau_Y)}\left[\mathbf{y}_{t+1}-F(\mathbf{y}_t,\mathbf{u}_t)_1\right] \tag{4}$$

Note that forward model F is first pre-trained and it is *not* optimized together with the dynamics cycle-consistency objective, as otherwise G and F can learn to map everything to zero so that $L_{\mathrm{dyn\_cyc}}$ becomes zero, which leads to trivial solution. Consequently, our full objective is:

$$\mathcal{L}_{\mathrm{full}}=\lambda_0\mathcal{L}_{\mathrm{dyn\_cyc}}(G,H)+\lambda_1\left(\mathcal{L}_{\mathrm{adv}}(H,D_U)+\mathcal{L}_{\mathrm{adv}}(P,D_A)+\mathcal{L}_{\mathrm{dom\_cyc}}(H,P)\right)+\lambda_2\mathcal{L}_{\mathrm{adv}}(G,D_Y) \tag{5}$$

where λ_0,λ_1 and λ_2 are constants balancing the losses.

There are several different specific application setting for this Cycle Dynamics Model. The first one is *cross-physics* (Figure 1(a)) where the observations are in the same modality but some physical parameters in the two domains are different. The second one is *cross-modality* (Figure 1(b)) where we want to align image observation and state observation in a self-supervised way. The third one is *cross-modality–and-physics* where both the observations and the dynamics are different, as shown in Figure 1(c)). This joint model can also be applied with two different morphology agents (*cross-morphology*). More detailed task introduction and the optimization strategy can be found in the Appendix A. Although there are four different settings, we only present the experiment results for two of them: *cross-modality* and *cross-morphology* in this paper.

4 Simulation Experiments

We first test the efficiency of our framework and conduct ablation studies in simulation environments. We choose MuJoCo physics simulator as our test bed. We model domain X and Y as two different environments, where input modality and morphology structures of the agents can vary. In the first part experiment, it is followed cross-modality alignment setting, where only the observation space is different; In the second part one, it is followed cross-morphology setting, where agent structures in two domains are different. Environment introduction, dataset collection, model implementation and the detailed settings can be found in the Appendix B.

Tasks	$L1$ Error ↓			RL Score ↑				
	Random	Cycle-GAN	Ours	Oracle, Y	Random, X	Cycle-GAN	Ours, $Y \to X$	Oracle, X
HalfCheetah	2.18	2.07	**0.57**	$6270_{\pm 123}$	$-289_{\pm 81}$	$-119_{\pm 65}$	**1504±256**	$3689_{\pm 247}$
FingerSpin	1.61	1.92	**0.23**	$804_{\pm 89}$	$0_{\pm 0}$	$0_{\pm 0}$	**341±39**	765 ± 68
FetchReach†	0.87	0.94	**0.05**	100%	0%	0%	**92%**	100%

Table 1: **Evaluation of cross-modality alignment**, including L1 error of state estimation, and RL policy performance on the original domain Y and after transferring to domain X. †: Task successful rate is reported.

Tasks	Oracle, Y	Random	Cycle-GAN	INIT	Ours, $Y \to X$
Cheetah	$6270_{\pm 123}$	$-250_{\pm 59}$	$-43_{\pm 52}$	$-37_{\pm 60}$	**2471±382**
Swimmer	$366_{\pm 26}$	$-1_{\pm 4}$	$14_{\pm 5}$	$-15_{\pm 3}$	**204±56**

Table 2: **Cross-morphology**. Results on transferring RL policies.

Cross-modality alignment. In this setting, we use RGB images as observations in domain X and the internal state of agents as observations in domain Y, while keeping physics parameters the same. G is then essentially a state estimator. We execute *random* actions without pre-trained policies in both domains to obtain unpaired training trajectories. We compute $L1$-distance between the predicted states and the ground-truth states from simulator X (although we do not use them for training) as an evaluation metric. We also use RL performance as another metric: we train an RL policy in state space (domain Y), and test it in image space (domain X) by executing the predicted action based on estimated states from images. We compare with two baselines: a random projection baseline; a image-state Cycle-GAN baseline (see Appendix E for details). As shown in Table 1, our approach performs significantly better than the Cycle-GAN baseline in both $L1$ error and the RL scores, which shows the importance of incorporating the dynamics into the cycle.

Cross-morphology alignment. Evaluation on two domains with different morphology. We experiment with two tasks (see Appendix C): (i) domain Y with 2-leg HalfCheetah and domain X with 3-leg HalfCheetah; (ii) domain Y with 3-limb Swimmer and domain X with 4-limb Swimmer. In this setting, the unpaired trajectories are also *randomly* sampled and our model learns to align the observations and actions at the same time. Once the correspondence is found, we can transfer the RL policies from domain Y to X. We compare to two baselines: one is the Cycle-GAN to perform both state-state and action-action translations, the other is using our action repetition initialization strategy before training (INIT, see Appendix C). As shown in Table 2, our approach can still perform reasonably well without finetuning the policy while the baselines completely fail.

5 Real Robot Experiments

We use an xArm robot for the *cross-modality alignment* task. The goal is to estimate the simulation states (domain Y) given the real robot images (domain X), without any paired image-state data. We *do not* have access to the internal states of the real robot. We use an uncalibrated RGB camera to capture the videos of the robot movements. We collect the real robot videos by randomly executing end-effector positional control.

Method	Random	Smooth
Random G	0.30	0.18
Cycle-GAN (E)	0.18	0.21
Ours (E)	**0.025**	**0.033**
Ours (J)	0.031	0.044

Table 3: **Real robot results.**

We collect random trajectories in xArm simulator. The training set includes 11k triplets (image, action, next image) of the real robot. We collect two testing sets from the real robot: a) 1,000 samples of random movement (Table 3, 1st col.), and b) 100 samples of smooth movement (Table 3, 2nd col.).

We conduct experiments using either end-effector position or joint poses (7 joint positions) as observations in simulation. Note the action is defined by the *delta movement* of the end-effector, not the exact position of the end-effector. We measure the L1-distance between the predicted and ground-truth end-effector position for evaluation. We compared our method with Cycle-GAN baseline (Appendix E). As shown in Table 3, the results from Cycle-GAN is close to random and our method with dyanmics cycle-consistency achieves much lower state estimation error. Besides training with end-effector as observations (Ours (E)), we also use joint poses as observations (Ours (J)) which increase the difficulty on learning the correspondence. Even so, our results are still much better than Cycle-GAN with end-effector observations. We also visualize the translation results by rendering the states in simulation in Appendix F, and observes that our state estimation results are well aligned with the real robot video.

References

H. B. Ammar, E. Eaton, P. Ruvolo, and M. E. Taylor. Unsupervised cross-domain transfer in policy gradient reinforcement learning via manifold alignment. In *Twenty-Ninth AAAI Conference on Artificial Intelligence*, 2015.

M. Andrychowicz, F. Wolski, A. Ray, J. Schneider, R. Fong, P. Welinder, B. McGrew, J. Tobin, O. P. Abbeel, and W. Zaremba. Hindsight experience replay. In *Advances in neural information processing systems*, pages 5048–5058, 2017.

M. Andrychowicz, B. Baker, M. Chociej, R. Jozefowicz, B. McGrew, J. Pachocki, A. Petron, M. Plappert, G. Powell, A. Ray, et al. Learning dexterous in-hand manipulation. *arXiv preprint arXiv:1808.00177*, 2018.

A. Bansal, S. Ma, D. Ramanan, and Y. Sheikh. Recycle-gan: Unsupervised video retargeting. In *Proceedings of the European conference on computer vision (ECCV)*, pages 119–135, 2018.

K. Bousmalis, A. Irpan, P. Wohlhart, Y. Bai, M. Kelcey, M. Kalakrishnan, L. Downs, J. Ibarz, P. Pastor, K. Konolige, et al. Using simulation and domain adaptation to improve efficiency of deep robotic grasping. In *2018 IEEE International Conference on Robotics and Automation (ICRA)*, pages 4243–4250. IEEE, 2018.

G. Brockman, V. Cheung, L. Pettersson, J. Schneider, J. Schulman, J. Tang, and W. Zaremba. Openai gym. *arXiv preprint arXiv:1606.01540*, 2016.

S. Fujimoto, H. Hoof, and D. Meger. Addressing function approximation error in actor-critic methods. In *International Conference on Machine Learning*, pages 1582–1591, 2018.

A. Gupta, C. Devin, Y. Liu, P. Abbeel, and S. Levine. Learning invariant feature spaces to transfer skills with reinforcement learning. *arXiv preprint arXiv:1703.02949*, 2017.

J. Hoffman, E. Tzeng, T. Park, J.-Y. Zhu, P. Isola, K. Saenko, A. A. Efros, and T. Darrell. Cycada: Cycle-consistent adversarial domain adaptation. *arXiv preprint arXiv:1711.03213*, 2017.

S. James, P. Wohlhart, M. Kalakrishnan, D. Kalashnikov, A. Irpan, J. Ibarz, S. Levine, R. Hadsell, and K. Bousmalis. Sim-to-real via sim-to-sim: Data-efficient robotic grasping via randomized-to-canonical adaptation networks. In *Proceedings of the IEEE Conference on Computer Vision and Pattern Recognition*, pages 12627–12637, 2019.

G. Joshi and G. Chowdhary. Cross-domain transfer in reinforcement learning using target apprentice. In *2018 IEEE International Conference on Robotics and Automation (ICRA)*, pages 7525–7532. IEEE, 2018.

K. H. Kim, Y. Gu, J. Song, S. Zhao, and S. Ermon. Cross domain imitation learning. *arXiv preprint arXiv:1910.00105*, 2019.

T. P. Lillicrap, J. J. Hunt, A. Pritzel, N. Heess, T. Erez, Y. Tassa, D. Silver, and D. Wierstra. Continuous control with deep reinforcement learning. *arXiv preprint arXiv:1509.02971*, 2015.

M.-Y. Liu, T. Breuel, and J. Kautz. Unsupervised image-to-image translation networks. In *Advances in neural information processing systems*, pages 700–708, 2017a.

Y. Liu, A. Gupta, P. Abbeel, and S. Levine. Imitation from observation: Learning to imitate behaviors from raw video via context translation. *arXiv preprint arXiv:1707.03374*, 2017b.

X. B. Peng, M. Andrychowicz, W. Zaremba, and P. Abbeel. Sim-to-real transfer of robotic control with dynamics randomization. *2018 IEEE International Conference on Robotics and Automation (ICRA)*, May 2018.

L. Pinto, M. Andrychowicz, P. Welinder, W. Zaremba, and P. Abbeel. Asymmetric actor critic for image-based robot learning. *arXiv preprint arXiv:1710.06542*, 2017.

F. Sadeghi and S. Levine. Cad2rl: Real single-image flight without a single real image. *arXiv preprint arXiv:1611.04201*, 2016.

P. Sermanet, C. Lynch, Y. Chebotar, J. Hsu, E. Jang, S. Schaal, S. Levine, and G. Brain. Time-contrastive networks: Self-supervised learning from video. In *2018 IEEE International Conference on Robotics and Automation (ICRA)*, pages 1134–1141. IEEE, 2018.

L. Smith, N. Dhawan, M. Zhang, P. Abbeel, and S. Levine. Avid: Learning multi-stage tasks via pixel-level translation of human videos. *arXiv preprint arXiv:1912.04443*, 2019.

Y. Tassa, Y. Doron, A. Muldal, T. Erez, Y. Li, D. d. L. Casas, D. Budden, A. Abdolmaleki, J. Merel, A. Lefrancq, et al. Deepmind control suite. *arXiv preprint arXiv:1801.00690*, 2018.

M. E. Taylor and P. Stone. Transfer learning for reinforcement learning domains: A survey. *Journal of Machine Learning Research*, 10(Jul):1633–1685, 2009.

M. E. Taylor, P. Stone, and Y. Liu. Transfer learning via inter-task mappings for temporal difference learning. *Journal of Machine Learning Research*, 8(Sep):2125–2167, 2007.

J. Tobin, R. Fong, A. Ray, J. Schneider, W. Zaremba, and P. Abbeel. Domain randomization for transferring deep neural networks from simulation to the real world. *2017 IEEE/RSJ International Conference on Intelligent Robots and Systems (IROS)*, Sep 2017.

W. Yan, A. Vangipuram, P. Abbeel, and L. Pinto. Learning predictive representations for deformable objects using contrastive estimation. *arXiv preprint arXiv:2003.05436*, 2020.

T. Zhou, P. Krahenbuhl, M. Aubry, Q. Huang, and A. A. Efros. Learning dense correspondence via 3d-guided cycle consistency. In *Proceedings of the IEEE Conference on Computer Vision and Pattern Recognition*, pages 117–126, 2016.

J.-Y. Zhu, T. Park, P. Isola, and A. A. Efros. Unpaired image-to-image translation using cycle-consistent adversarial networks. In *Proceedings of the IEEE international conference on computer vision*, pages 2223–2232, 2017.

A Optimization and Tasks

Optimization. We collect unpaired trajectories τ_X and τ_Y by executing random actions from both domains. Directly optimizing the full objective end-to-end leads to model collapse, as it involves joint optimization with multiple neural networks: G and H can easily discover a "short-cut" solution, where the translated observations and actions are not valid but they can fool the forward model to optimize the dynamics cycle-consistency objective. Since the forward model is only optimized on trajectory data τ_Y, thus we first pre-train the forward model and fix its parameters throughout the following training procedure. We initialize the action mapping function using an algorithm detailed in the Appendix C.4. We propose to employ alternating training procedure for the full objective: When we train the observation mapping function G and its auxiliary discriminator D_Y, we fix the action mapping function H and P; then when the action mapping function H and P with D_U and D_A are trained, we fix the observation mapping function G. Since the action mapping functions are reasonably initialized, at the beginning of training procedure the observation mapping function is optimized. It is grounded on good action mappings, as well as the dynamics of environments by dynamics cycle consistency, thus it is constrained from learning an arbitrary short cut. Subsequently, action mapping functions can be further fine-tuned once we obtain a good observation mapping function (Algorithm 1).

Tasks. Our formation of correspondence learning is broad and general, and it enables many applications which typically require intricately designed frameworks or are hard to solve without paired data. Specifically, we study the following three tasks:

Algorithm 1: Alternatingly Joint Training Algorithm

Input: Domain X: $\tau_X = \{(\mathbf{x}_t, \mathbf{a}_t, \mathbf{x}_{t+1})\}$
Domain Y: $\tau_Y = \{(\mathbf{y}_t, \mathbf{u}_t, \mathbf{y}_{t+1})\}$
// Training Forward Model Stage
train $\mathcal{L}_{\text{forward}}(F)$ (Eq. 4) to learn transition dynamics T_Y in domain Y;
// Alternatingly Training Stage
for $i = 1$ *to* e **do**
  reset λ_1, set $\lambda_2 = 0$; fix weight of G;
  for $j = 1$ *to* e_1 **do**
    using $\mathcal{L}_{\text{full}}$ (Eq. 5) to train model H and P;
  reset λ_2, set $\lambda_1 = 0$; fix weight of H and P;
  for $j = 1$ *to* e_2 **do**
    using $\mathcal{L}_{\text{full}}$ (Eq. 5) to train model G;
return State alignment model G
Action alignment model H and P

The first task is *cross-physics* alignment, where domain X and domain Y are two environments with different *physics parameters* but same input modality. As shown in Figure 1(a), same input modality indicates that observation correspondence always holds, i.e., $\mathbf{x}_t \equiv \mathbf{y}_t$; different physics parameter indicates that executing a same action at the same initial observation in separate environments results in different next observation. After learning correspondences, assuming we have a policy in domain Y, we can transfer it to domain X by mapping the predicted action of the policy $\mathbf{u}$ from domain Y to X with action mapping function P. The translated action $\tilde{\mathbf{a}}$ can then be executed in domain X.

The second task is *cross-modality* alignment, where domain X and domain Y are different sensing (observation) modality of the *same* agent, which implies that action correspondence between two domains always hold (see Figure 1(b)). In other words, H and P are both identity mapping, and $\mathbf{a}_t \equiv \mathbf{u}_t$. Thus we can set $\gamma = 0$ in Eq. 5 in training. A predominant choice is X being image while Y being state, where G essentially learns to perform state estimation. Moreover, we can execute a policy which is originally trained on *state space* in *image space*, as the input $\mathbf{x}_t$ in image space can be translated by G before fed into the policy based on state space, yielding a predicted action $\mathbf{u}_t$, which can be directly executed in domain X.

Combining the above-discusses two tasks yields the third task, in which cross-physics and cross-modality alignment are realized simultaneously, thanks to our proposed joint alternative training procedure. We refer to it as *cross-modality-and-physics* alignment, as shown in Figure 1(c). This formulation can be further extended to another task, where domain X and Y are two agents with different morphologies, termed as *cross-morphology* alignment. For example, domain X can be a three-leg cheetah and domain Y can be a two-leg cheetah. In this case, the representations of $\mathbf{x}$ / $\mathbf{y}$ and $\mathbf{a}$ / $\mathbf{u}$ are fundamentally different, yet intrinsically they share similarities in locomotion.

As the correspondence is established between two domains, it can be applied to different downstream applications. Suppose that our goal is to transfer a policy trained in domain Y to X. Inference includes three steps: (i) Given an observation $\mathbf{x}_t$ in domain X, use observation mapping function G to translate $\mathbf{x}_t$ to $\mathbf{y}_t$; (ii) Execute the policy in domain Y given $\mathbf{y}_t$, and obtain the action output $\mathbf{u}_t$; (iii) Translate the action $\mathbf{u}_t$ from domain Y back to domain X with the action mapping function P.

B Simulation Experiment Details

We believe that our method can be applied to a lot of environments. However, in this paper we focus on the representative ones including two tasks based on OpenAI Gym [Brockman et al., 2016], i.e., "HalfCheetah", "FetchReach" and one task based on DeepMind Control [Tassa et al., 2018], i.e., "FingerSpin". To sample the training data, we randomly collect $50k$ unpaired trajectories in both domain X and domain Y in most settings. The evaluation dataset size is $10k$. Besides evaluating on the alignment errors, we also benchmark how well the pre-trained RL policies in one domain can be transferred to another domain. To pre-train the policy, we use DDPG [Lillicrap et al., 2015] with HER [Andrychowicz et al., 2017] for "FetchReach" and TD3 algorithm [Fujimoto et al., 2018] for other environments. Note that we do *not* need to further fine-tune the policy for transferring to a new domain. We report the task success rate for "FetchReach" and task rewards for the other environments. All RL policies are trained with 5 different seeds. Here we present more details about our method implementation and the reference policies.

B.1 Network Architecture

The network architectures for each separate settings are as follows:

Cross-physics. The discriminator D is a five-layer MLP (hidden size: 32, 64, 128, 32) which takes states as input and predicts whether a state is true or fake. The forward dynamics model F is a four-layer MLP (hidden size: 64, 128, 32) which takes current state and action as input and predicts the next state. The observation alignment function G is an identity mapping. The action alignment functions H and P are MLPs (hidden size: 32, 64, 128, 32) which take current state and action as input and predicts corresponding action in the other domain.

Cross-modality. The discriminator D and the forward dynamics model F are the same as that in the "cross-physics" setting. The observation alignment function G is a ResNet-18 and followed by an MLP head (hidden size: 256, 64, 32) which outputs corresponding state. The action alignment functions H and P are identity mapping.

Cross-morphology. Newtorks D, F, H and P are the same as that in the "cross-physics" setting. The observation alignment function G is the same as that in the "cross-modality" setting.

B.2 Training

Given the dataset of unpaired and unaligned samples from two domains, we first train the forward dynamics model F on domain Y until it converges, we use Adam optimizer [**?**] with initial learning rate 0.001 which is decreased by half every three epochs and train the network for 20 epochs. This is the same for all the settings. Secondly, we train the action alignment functions H, P or observation alignment function G by optimizing Eq. 5. The pipeline and optimization chain for each separate settings are as follows:

Cross-physics. We optimize the alignment functions H, P here. We set $\lambda_0 = 200$, $\lambda_1 = 1$, and $\lambda_2 = 0$ in Eq. 5, where $\lambda_2 = 0$ means we are not using the observation alignment function G. Note that although the forward dynamics model F is involved in the back-propagation, we are fixing the weights of F. We train the models by using the Adam optimizer for 50 epochs with a batch size of 32. The learning rate is set to 0.001 and decreased by $1/3$ for every 10 epochs.

Cross-modality. We optimize the observation alignment function G. We set $\lambda_0 = 200$, $\lambda_1 = 0$, and $\lambda_2 = 3$ in Eq. 5, where $\lambda_1 = 0$ means we are not using the action alignment function H, P. Similarly, the forward dyanmics model F is freezed. We train the model with Adam for 50 epochs with a batch size of 32. The learning rate is set to 0.001 and decreased by $1/3$ for every 10 epochs.

Cross-morphology (Joint training). Networks H, P, and G are optimized by Adam optimizer while the forward dyanmics model F is freezed. We combine the training procedure in cross-physics

and cross-modality settings following Algorithm 1. The model is trained for 10 epochs with a batch size of 32. The training alternates every 5000 steps (e1 and e2). Note each epoch contains more training steps in joint training. The learning rate is set to 0.0001.

B.3 Reference Policy

We use DDPG [Lillicrap et al., 2015] with HER [Andrychowicz et al., 2017] for "FetchReach" and TD3 [Fujimoto et al., 2018] for other environments. For DDPG, we train the policy for 50 epochs of 400 episodes in each epoch. The policy exploration epsilon ratio is 0.3 and the reward discount factor is 0.98. For TD3, we train the policy for 400k time steps. The initial exploration step is 25k. The reward discount factor is 0.99, the target network update rate is 0.005 and exploration noise standard deviation level is 0.1. When evaluating the performance of the policies, we calculate 50 episode rollout rewards across 5 different seeds. We report the rewards with variance in all tables.

C Experiment Setting

C.1 Cross-physics agent setting

The physical parameters in cross-physics settings are shown in Table 4. The "Parameter" column represents which type of parameter is changed in each task. Recall that we train the RL policy in domain Y and evaluate in domain X in our evaluation. The numbers in the columns of domain X and domain Y are the physics values for each domain. The physics parameter in domain Y is defined by default in the OpenAI Gym MuJoCo simulation environment. The physics parameter in domain X is selected so that it can cause obvious distortion to the policy trained in domain Y (as shown in Table **??**). Note that we did *not* perform physics parameter search for improving our method. For the domain randomization baseline, the parameter value for each episode is uniformly sampled from the range shown in the last column.

Parameter	Envs	Domain X	Domain Y	DR Range
Armature	HalfCheetah	0.3	0.1	[0.2, 0.4]
	FingerSpin	2.0	0.0	[1.0, 3.0]
	FetchReach	3.0	1.0	[2.0, 4.0]
Torso Mass	Walker	0.4	1.0	[0.0, 0.8]
	Hopper	1.2	1.0	[0.8, 1.6]

Table 4: **Cross_physics physical hyperparameter settings.** The parameters in domain X, domain Y and parameter range for domain randomization baseline for each task.

C.2 Cross-modality agent setting

In this setting, the resolution of the image observation in domain X is 256×256 and we concatenate three images (current and previous two frames) as the observation input for G to estimate the state. By concatenating multiple images instead of one, it allows the representation to capture the velocities and motion of the agent, which is a common practice for vision-based RL.

C.3 Cross-morphology agent setting

We introduce two tasks for the cross-morphology experiments including the "HalfCheetah" and "Swimmer" environments. As shown in Figure 2, for "HalfCheetah", we modify the agent by adding one more hind leg of the same structure as the original hind leg to obtain a three-leg cheetah. For "Swimmer", we add one more limb cloned from the original third limb, leading to a four-limb swimmer.

C.4 Initialization for Action Alignment Model

In the cross-modality-and-physics alignment, for agents with the same morphology and structure, we initialize the action translation between two domains by identity mapping, and only train the

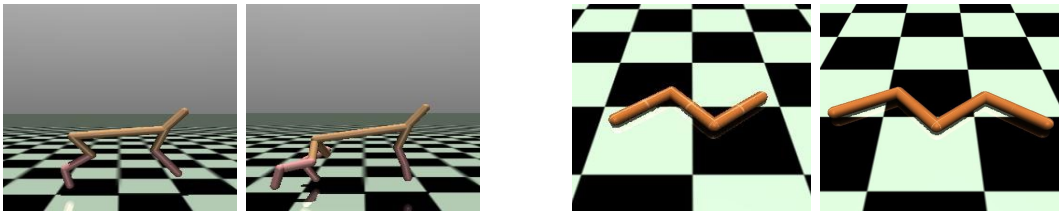

Figure 2: **Cross-morphology agent introduction.** Left: two-leg Cheetah and its three-leg counterpart. Right: three-limb swimmer its four-limb counterpart. *Please check out our supplementary video for visualization.*

observation alignment model (G) in the beginning. Then we unfreeze the action alignment model (H and P) and jointly train all models by our alternative training procedure.

For agents of different morphology (e.g., different number of limbs and joints), the dimensions of action spaces are naturally different. Thus it is impossible to initiate action mapping functions with identity mapping. Note that we can still use identity mapping for the original joints and limbs between two domains. For extra joints and limbs, we borrow the mapping function from nearby joints to initialize the novel joints. For example, in our experiments, we can find correspondence between the three-leg cheetah and the two-leg cheetah. For the newly-added leg, we use and repeat the nearby original hind leg actions to initialize its actions. There is no correspondence established from this initialization, as shown by the experiment results—we provides this initialization baseline for cross-morphology policy transfer in Table 2. This baseline perform much worse than our approach.

D Implementation details

D.1 Network Architecture

The network architectures for each separate settings are as follows:

Cross-physics. The discriminator D is a five-layer MLP (hidden size: 32, 64, 128, 32) which takes states as input and predicts whether a state is true or fake. The forward dynamics model F is a four-layer MLP (hidden size: 64, 128, 32) which takes current state and action as input and predicts the next state. The observation alignment function G is an identity mapping. The action alignment functions H and P are MLPs (hidden size: 32, 64, 128, 32) which take current state and action as input and predicts corresponding action in the other domain.

Cross-modality. The discriminator D and the forward dynamics model F are the same as that in the "cross-physics" setting. The observation alignment function G is a ResNet-18 and followed by an MLP head (hidden size: 256, 64, 32) which outputs corresponding state. The action alignment functions H and P are identity mapping.

Cross-morphology. Newtorks D, F, H and P are the same as that in the "cross-physics" setting. The observation alignment function G is the same as that in the "cross-modality" setting.

D.2 Training

Given the dataset of unpaired and unaligned samples from two domains, we first train the forward dynamics model F on domain Y until it converges, we use Adam optimizer [**?**] with initial learning rate 0.001 which is decreased by half every three epochs and train the network for 20 epochs. This is the same for all the settings. Secondly, we train the action alignment functions H, P or observation alignment function G by optimizing Eq. 5. The pipeline and optimization chain for each separate settings are as follows:

Cross-physics. We optimize the alignment functions H, P here. We set $\lambda_0 = 200$, $\lambda_1 = 1$, and $\lambda_2 = 0$ in Eq. 5, where $\lambda_2 = 0$ means we are not using the observation alignment function G. Note that although the forward dynamics model F is involved in the back-propagation, we are fixing the weights of F. We train the models by using the Adam optimizer for 50 epochs with a batch size of 32. The learning rate is set to 0.001 and decreased by $1/3$ for every 10 epochs.

Cross-modality. We optimize the observation alignment function G. We set $\lambda_0 = 200$, $\lambda_1 = 0$, and $\lambda_2 = 3$ in Eq. 5, where $\lambda_1 = 0$ means we are not using the action alignment function H, P. Similarly, the forward dyanmics model F is freezed. We train the model with Adam for 50 epochs with a batch size of 32. The learning rate is set to 0.001 and decreased by $1/3$ for every 10 epochs.

Cross-morphology (Joint training). Networks H, P, and G are optimized by Adam optimizer while the forward dyanmics model F is freezed. We combine the training procedure in cross-physics and cross-modality settings following Algorithm 1. The model is trained for 10 epochs with a batch size of 32. The training alternates every 5000 steps (e1 and e2). Note each epoch contains more training steps in joint training. The learning rate is set to 0.0001.

D.3 Reference Policy

We use DDPG [Lillicrap et al., 2015] with HER [Andrychowicz et al., 2017] for "FetchReach" and TD3 [Fujimoto et al., 2018] for other environments. For DDPG, we train the policy for 50 epochs of 400 episodes in each epoch. The policy exploration epsilon ratio is 0.3 and the reward discount factor is 0.98. For TD3, we train the policy for 400k time steps. The initial exploration step is 25k. The reward discount factor is 0.99, the target network update rate is 0.005 and exploration noise standard deviation level is 0.1. When evaluating the performance of the policies, we calculate 50 episode rollout rewards across 5 different seeds. We report the rewards with variance in all tables.

E Details of Cycle-GAN Baselines

Here we introduce the details of Cycle-GAN baseline for each different settings.

Cross-physics. In this setting, the Cycle-GAN baseline translates actions between two domains. The generators and discriminators are MLPs and the cycle loss is the L1 loss. The MLP network structures follow our approach. The results show that the policy fails to perform across domains and the mapping is close to random, so we have not included this baseline in the table.

Cross-modality. In this setting, the Cycle-GAN baseline translates between image and its corresponding state. The image-to-state generator is the same as G. The state-to-image generator is composed of MLPs and six upsampling blocks. Each block consists of one transposed convolution layer, one BatchNorm layer and one ReLU activation layer. The cycle loss is L1 loss. This setting is also applied to our real robot experiment.

Cross-morphology. The Cycle-GAN model translates states and actions between two domains. All generators and discriminators are MLPs and the cycle loss is L1 loss.

We visualize in Figure 3 the learned correspondence from the **cross-modality alignment** on the HalfCheetah experiment, where observations of images are translated to states. In each plot, x-axis represents the true-state of the image and the y-axis represents the translation result from the network. Each point in the plot represents a random sample. We can see that our method is able to translate the image to the correct states as most of the dots are in the diagonal line ($y = x$), while Cycle-GAN yield near random translation similar to the random baseline. The result underlines the significance of incorporating dynamics into cycle-consistency.

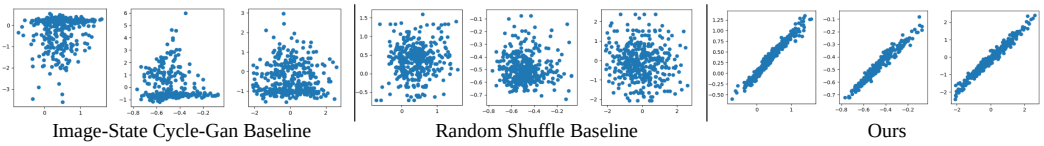

Figure 3: **Correspondence visualization for Cycle-GAN baseline and ours.** Cycle-GAN model performs nearly the same as the random shuffle baseline while our model can correctly find the correspondence between the image modality and the state modality.

The qualitative visualizations for Cycle-GAN and ours are shown in Figure 4 for the **cross-modality alignment** on HalfCheetah. These five sub-figures from left to right in sequence are as follows: (a) One random image observation sample from the dataset. (b) The rendered image from the state which is predicted by Cycle-GAN model. (c) The rendered image from the state which is predicted by our model. (d) The image with a new renderer for our model prediction, giving a different rendering view

of the state. (e) The training curve of L1 error for self-supervised state estimation. After training, our model output is almost the same as the ground-truth while the Cycle-GAN model completely fails.

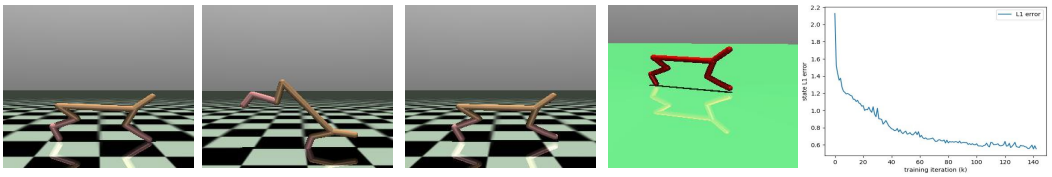

(a) Random sample (b) Cycle-GAN (c) Ours (d) New render (e) Training curve

Figure 4: **Qualitative visualization for Cycle-GAN baseline and ours.** The rendered image (c) from our model prediction looks almost the same like the original input image (a) while Cycle-GAN baseline (b) fails. The last small figure visualizes the L1 error between the ground-truth state and our model prediction during the training process and proves the effectiveness of our method in self-supervised state estimation. More visualizations are presented in the project page link given in the abstract.

F Real Robot Qualitative Visualizations

The real robot experiment qualitative visualizations are shown in the following figure.

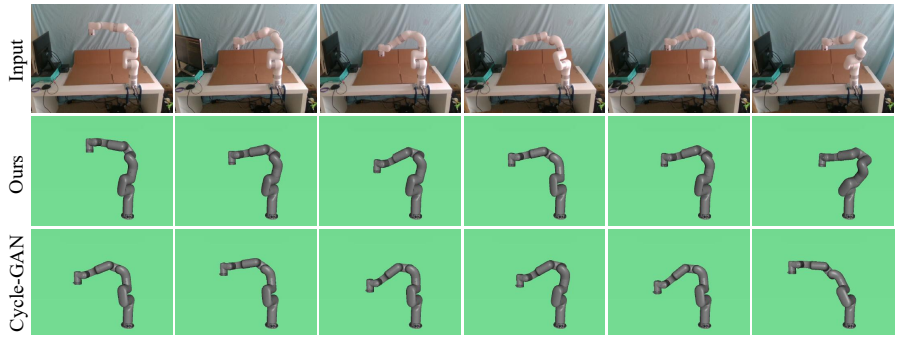

Figure 5: **Visualization** of learnt correspondence from RGB images to robot joint states with xArm robot. We render the predicted states in simulation with green background. While Cycle-GAN struggles to find the correct correspondence, the results of our method highlights the importance of dynamics cycle-consistency objective. (Best viewed in Adobe Acrobat to see the gif of the last column.)

G Discussions

G.1 No compounding error

Compouding error issue is a common problem in robotics. However, our model can alleviate this error: during inference in X domain, every time step we obtain a new state in X, we will translate it to Y domain for the RL policy to decide the action. If the agent is off the track, the RL policy will be able to recover it. The translated state for RL agent is bounded by the discriminator. These alleviate the compounding error issue.

G.2 Time Contrastive Networks

The Time Contrastive Networks (TCN) proposed by Sermanet et al. [2018] have three limitations and thus it is not applicable in our setting: (i) It can not estimate the state directly from the image; (ii) It requires paired data from two domains for learning encoded feature, while our approach is trained in the unpaired data setting; (iii) Since the data from two domains share the same TC embedding network, it can not be used to align different modalities.